WWW.IJRPR.COM

International Journal of Research Publication and Reviews

Journal homepage: www.ijrpr.com ISSN 2582-7421

Studies On Modification Of Defects And Disorder In Carbon Nanostructures

YASSAR PARVEZ ROUNYAL

Bhagwant university Ajmer

ABSTRACT :

Carbon is one of the most prevalent elements on earth and the basis of all the life. It exhibits a variety of hybridizations, including sp, sp2, and sp3, due to its electronic configuration 1s22s22p2. Graphite and diamond are well known crystal structures of carbon. Diamond has sp3 hybridized carbon, covalently bonding in tetrahedral co-ordination. Graphene, carbon nanotubes, fullerenes, and carbon black are a few of the other sp2 hybridized (graphitic carbon) carbon materials. Graphene is one atomic thick monolayer of carbon atoms arranged in two dimensional honeycomb lattice and is the building block of graphite. Carbon nanotubes (CNT) are one dimensional allotrope of carbon and made of rolled up graphene sheet into cylindrical shape. Carbon black (CB) consists of sp2 hybridized carbon layers that are roughly parallel to each other but randomly rotated along the c-axis with lot of stacking faults, and belongs to a turbostratic graphitic structure.

All these carbon materials in their pristine form possess very interesting properties and thus applications. A 'defect' is defined as any kind of local disruption to the crystalline order in materials. According to thermodynamics, completely defect-free materials do not exist. In general, defects in materials are undesired as they affect the material's properties and thus their applications. Mechanical, optical, chemical and electronic properties of materials are susceptible to be changed with the defect concentration present in them. Some of the disordered carbon materials are believed to be the desirable candidates for anodes of secondary lithium-ion batteries. Further, the presence of structural defects play an important role in the graphite-to-diamond transformation. Thus, introduction/alteration of defects in carbon nanomaterials is an interesting way to tailor their properties.

Keyword: Carbon Nanostructures, Graphene, Carbon Nanotubes (CNTs), Defect Engineering, Disorder Modification, Raman Spectroscopy etc.

1. INTRODUCTION:

Carbon nanostructures, such as graphene and carbon nanotubes (CNTs), have garnered
significant attention due to their exceptional electrical, thermal, and mechanical properties. These materials have shown immense potential in various applications, including electronics, energy storage, composites, catalysis, and biomedicine. However, the presence of defects and disorder within these structures can drastically influence their properties, presenting both challenges and opportunities for material scientists.

1.1 Carbon and its allotropes:

Carbon is among the most abundant element on earth and the basis of all life. Due to the electronic configuration $1s^2 2s^2 2p^2$ it exhibits a variety of hybridizations, including sp, sp^2, and sp^3 [2]. It forms various allotropes with these different hybridization states, such as diamond with sp^3 hybridization, graphite with sp^2 hybridization, and carbyne with sp hybridization. Among these, the well-known crystal structures of carbon are graphite and diamond [1,2] which are extensively studied both theoretically and experimentally. Other sp^2 hybridized (graphitic carbon) materials include graphene, carbon nanotubes, fullerenes, carbon black, etc. [2,3]. The building block of these nanostructured graphitic carbon materials is graphene, which is a single sheet of graphite with a hexagonal atomic arrangement.

1.1.1. Diamond:

Diamond is a sp^3 hybridized carbon allotrope and is known as the hardest material, having a bulk modulus of about 430 GPa [4]. In diamond, every carbon atom forms four covalent bonds and exists in the tetrahedral coordination, as shown in **Fig. 1.1 (a)**. It usually crystallizes in cubic structure and belongs to Fd3̄m space group, with the C—C bond length of 1.54Å and C—C—C bond angle of 109.47°. The density of diamond is 3.5 g/cc. However, diamond can also be found in hexagonal structure called hexagonal diamond or lonsdaleite. These two polytypes differ in the stacking style of the carbon layers.

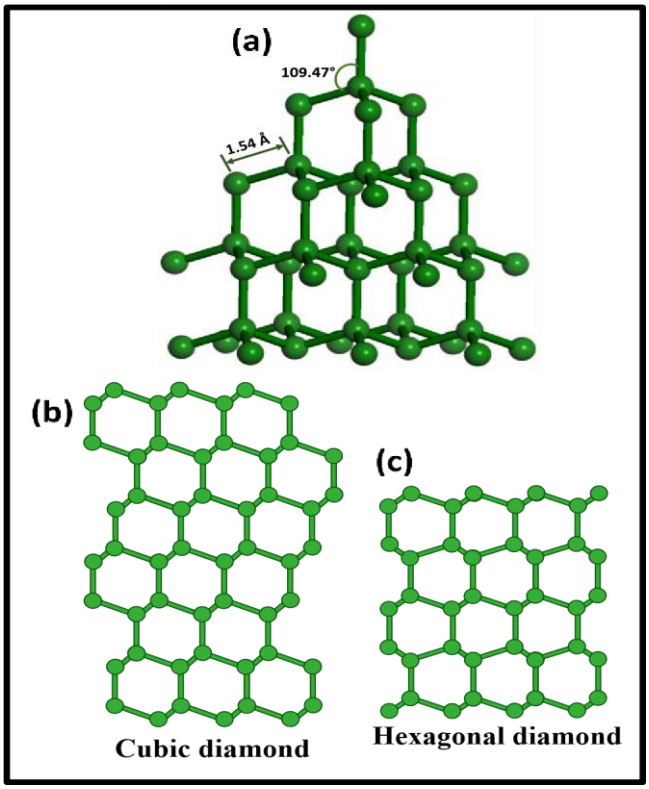

Fig. 1.1: A ball-stick schematic representation of the cubic diamond structure (a). Images depicting the stacking sequence of layers in cubic diamond (b) and hexagonal diamond (c).

Diamond covers a broad spectrum of properties such as high thermal conductivity (>2000 $Wm^{-1}K^{-1}$), wide electronic energy bandgap (~ 5.5 eV, which means high electrical insulation), high wear resistance, and high hardness (Mohs scale hardness value of 10), low coefficient of thermal expansion ($0.7x10^{-6}$ K^{-1}), chemical inertness, and low absorption to visible radiation [7, 8]. Owing to its wide range of properties, diamonds are extensively used in several applications such as abrasives, as gems in jewelry, cutting tools, and heat sinks. Diamonds are also used in engineering applications such as indenting probes to check the hardness of materials, etc.

1.1.2. Graphite:

Graphite is the most stable bulk allotrope of carbon at ambient conditions. It has a layered structure in which carbon atoms are arranged in a honeycomb lattice with sp^2 hybridization. Each carbon atom forms three covalent bonds in graphite and exists in trigonal coordination. These carbon layers in graphite are called graphene sheets. The carbon atoms within the layer interact through covalent bonding, whereas interlayer atoms are held through weak Van der Waals interactions. Graphite belongs to $P6_3/mmc$ space group and crystallizes in hexagonal structure with four atoms per unit cell. The lattice parameters of graphite are a=2.46 Å and c=6.71 Å, and the interlayer separation is 3.35 Å. The density of graphite is 2.27 g/cm^3. The graphene layers in the graphite have ABAB… stacking sequence. The structure of graphite is shown in **Fig. 1.2**. Graphite exhibits good electrical conductivity (10^3 Scm^{-1}), chemical inertness, good thermal conductivity (~ 2000 $Wm^{-1}K^{-1}$), etc.

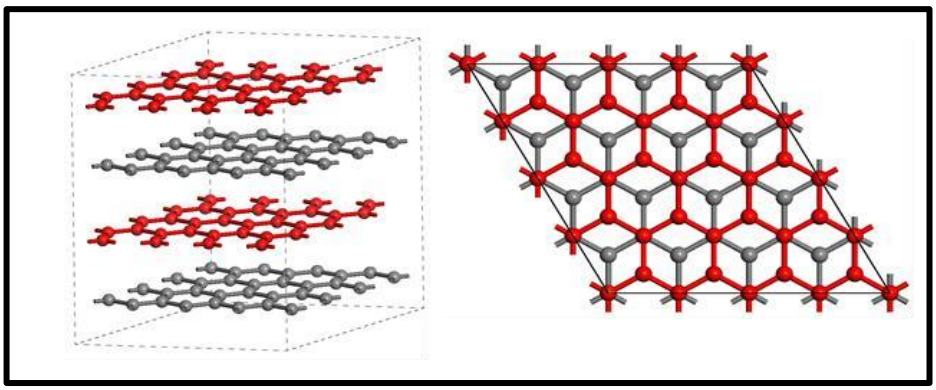

Fig. 1.2: A ball-stick schematic representing the layered structure of Bernal stacked graphite with side view (left) and top view (right).

Due to good electrical conductivity, graphite is used as electrode material in Li-ion batteries and also in the fabrication of electromagnetic interference shielding materials. Since the individual layers in graphite are held through weak Van der Waals bonding, they easily slip over others, enabling them to be used in dry lubricants and pencils.

1.1.3. Carbon Nanotubes (CNTs):

Carbon nanotubes are cylindrical structures made from rolled-up sheets of graphene. They can be single-walled (SWCNTs) or multi-walled (MWCNTs), depending on the number of graphene layers rolled into the tube. CNTs have exceptional mechanical strength, electrical conductivity, and thermal conductivity.

Carbon nanotubes (CNTs) were first found by S. Ijima in 1991 under a transmission electron microscope while characterizing carbon soot arc-discharge synthesis used for fullerene production. Carbon nanotubes are two types, single-walled carbon nanotubes (SWCNTs) and multiwalled carbon nanotubes (MWCNTs). CNT can be thought as a graphene sheet rolled up into the shape of a cylinder with a typical diameter of a few nanometers and a length up to a few micrometers (**Fig. 1.3**). SWCNT is a single graphene sheet wrapped into the shape of a seamless cylinder. On the other hand, MWCNTs are co-axial cylinders whose basic unit is a SWCNT. The separation between two tubes is about 3.38Å and comparable to the interlayer separation in graphite. CNTs can be synthesized using different methods such as arc-discharge method, chemical vapor deposition method, laser ablation method, etc.

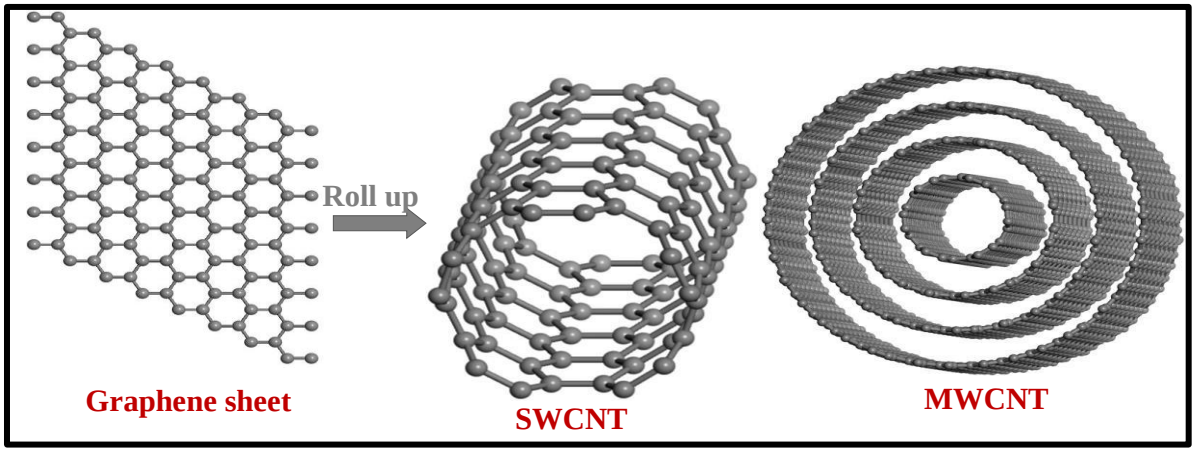

Fig. 1.3: Schematic image depicting the graphene sheet, single and multi-walled carbon nanotubes.

Due to their nanostructure, CNTs exhibit some peculiar properties. They are highly conducting ($8x10^8$ Scm^{-1}), super strong, possess high thermal conductivity (3000 $Wm^{-1}K^{-1}$), are stable up to very high temperatures (4000K), and have exceptional mechanical properties. The most interesting property of these nanotubes is their high surface-to-volume ratio, which enables them as an appropriate candidate material to be used in sensor applications. The CNTs can be metallic or semiconducting, depending on how they are rolled. Their unique properties make them suitable for applications in nanotechnology, electronics, materials science, and medicine CNTs have a wide range of applications, such as catalyst support, energy conversion catalyst, biosensors etc.

1.1.4. Amorphous carbon:

Amorphous carbon is a form of carbon that does not have a crystalline structure. It includes carbon black, soot, and activated carbon. Amorphous carbon materials are used in a variety of applications, including as pigments, in filtration, and as electrodes in batteries.

Recently, amorphous carbon is also considered as one of the carbon allotropes. It is a nanostructured material, and as the name suggests, the carbon atoms in it do not have any longrange order, and only short-range ordering exists. **Fig. 1.4** depicts the structure of the amorphous carbon. Carbon atoms in amorphous carbon do not possess any unique hybridization, rather they have different fractions of all the possible hybridization states (sp, sp^2, and sp^3). There exists disorder in bond lengths and bond angles in amorphous carbon, and it consists of a high concentration of dangling bonds. Depending on the preparation methods and conditions, the properties of amorphous carbon vary. Some important properties of amorphous carbon are high mechanical hardness, chemical inertness, and high thermal conductivity.

Fig. 1.4: Ball and stick representation of structure of the amorphous

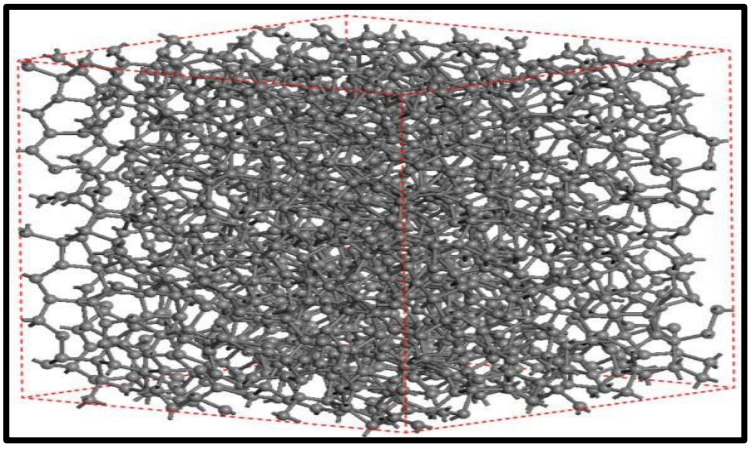

Amorphous carbon with high sp^3 hybridization is called tetrahedral amorphous carbon or diamond-like carbon. Amorphous carbon functionalized with hydrogen is called hydrogenated amorphous carbon. The usage of amorphous carbon materials in applications like protective tribological coating, radiation protection, and electron field emitters is well reported.

1.1.5 Fullerenes:

Fullerenes are molecules composed entirely of carbon, taking the form of a hollow sphere ellipsoid, or tube. The most well-known fullerene is C60, also known as buckminsterfullerene or buckyballs, which resembles a soccer ball made of 60 carbon atoms. Fullerenes have unique electronic, thermal, and structural properties, making them useful in materials science, electronics, and nanomedicine.

1.2. Defects and their effect on carbon nanostructures:

A 'defect' in a crystalline material is defined as any kind of local disruption to the crystalline order. A completely defect-free crystalline solid is an idealization which does not exist in nature. Therefore, materials inevitably consist of defects. Common type of defects found in materials are grain boundaries (edges), vacancies, interstitials, dopant atoms (hetero/homo), etc. In general, defects in materials are undesired as they affect the material's properties and thus their applications. Mechanical, optical, chemical and electronic properties of materials are susceptible to be changed with the defect concentration present in them. However, the manner in which the defects presence manifests itself onto the usefulness of a material's properties is rather subjective and is not always detrimental. It has been discovered that in certain cases the existence of faults in materials is beneficial and leads to improved performance of materials. It is known that the single crystals with almost defect-free structures have weaker mechanical properties than polycrystalline ones since the interaction between defects and grain boundaries is strong in the latter. Indeed, it has been proposed that materials such as metals and semiconductors having defects are more intriguing and possess useful properties than their perfect crystalline counterparts. It is also well known that adding impurities into the metals results in formation of alloys with exceptional strength and corrosion resistance. Famously known Si, and Ge are intrinsic semiconductors which requires introduction of defects in the form of atomic doping of n- or p-type impurity elements in order to make them useful for semiconductor devices applications

1.2.1. Defects in graphitic carbon materials:

Graphene is main basic unit of all the graphitic carbon materials, and it suffers mainly from nonhexagonal rings/pair of 5/7 rings (Stone-Wales defects), single vacancy defects, multiple vacancy defects, line defects, carbon adatoms, cluster defects, and boundaries. The common defects observed in CNTs are point defects (vacancies, interstitials), bond rotations and StoneWales defects, dopants and adatoms. Point defects, dislocations, grain boundaries and impurities are the common type of defects in graphite. The defects form in these graphitic materials while their synthesis and growth, and they can also be introduced via particle irradiation such as electron and ion irradiation.

1.2.2. Influence of defects on graphitic carbon nanomaterials:

Though defects carry a negative connotation, they are proved to be useful in certain cases even in graphitic carbon materials. For example, presence of edge defects is found to aid in promoting electrocatalytic activity of graphene. The oxygen reduction reaction (ORR) performance of defect induced graphene via Ar plasma etching is reported to be greater as compared to the pristine graphene. Graphene sheets with high density of large-angle tilt boundaries have shown better mechanical strength as compared to those with low-angle boundaries having less defects. Ndoped, S-doped, and P-doped graphene is found to exhibit superior electrocatalytic performance as compared to its pristine counterpart. It is also reported that the capacitance of supercapacitors based on N-doped graphene was increased by four folds in comparison with pristine graphene based device. It is very clear from the theoretical studies that the vacancies present in graphene are responsible for the induction of magnetic order in it. It is found that the introduction of hetero-atoms such as nitrogen greatly enhances the chemical reactivity of graphene.

Further, the presence of defects in CNTs is known to result in their better adhesion to a polymer matrix which in turn results in improved composite mechanical characteristics. Introduction of defects in CNTs is found to result in their enhanced filed emission property and mechanical strength. Stone-Wales defects are reported to be crucial in joining the semiconducting nanotube to a metallic one to make a nanodiode for the design of nanoelectronics. Structural defects in MWCNTs are found to increase their electrical conductivity due to the formation of conductive interlayer cross-linkings mediated by these defects. It is further known that, highly defective MWCNTs are desirable candidates in sensor applications, hydrogen storage, field emission devices, and lithium intercalation applications. Tao et al. also reported the enhanced ORR performance of defective CNTs as compared to the pristine one. B-doped carbon nanotubes offers. electrocatalytic performance as compared to the pristine carbon nanotubes. Introduction of vacancy defects in semiconducting SWCNTs is found to decrease their bandgap. Defects in SWCNTs are shown to dramatically enhance their photoluminescence intensity. It is known that the vacancy defects in graphite results in alteration of its thermal and electrical conductivity. Wang et al., were successful in improving the fast charging capacity of graphite anodes used in Li-ion batteries via defect engineering in graphite based on a thermal treatment of graphite in CO_2 gas. It is found that introduction of intrinsic defects into the graphite by CO_2 treatment results in improved kinetics of lithium ion intercalation that in turn increases rate of charging of graphite anodes. The vacancy defects introduced into the graphite by ball milling is found to enhance its sodium/lithium storage capacity, which is helpful in the field of sodium ion and lithium ion batteries.

There is a plethora of literature reporting the presence of defects and their effects on the properties of graphitic carbon materials. The above listed reports are some of them. However, the noteworthy observation here is that the properties associated with these defects can affect the graphite materials in such a way that a few enhanced and sometimes seemingly contrasting attributes maybe introduced to the graphitic lattice which is otherwise defect-free. Following are the few important and intriguing effects induced by defects in graphitic carbon materials:

- Intrinsic defects in graphitic carbon nanostructures are found to modify the electronic structure of these materials locally and lead to the creation of localized electronic states and also result in their enhanced chemical activity, similar to dangling bonds. It is also known that the dangling bonds around the structural defects result in formation of interlayer covalent bonds which in turn leads to the creation of large regions of sp^3 hybridized atoms inside the sp^2 hybridized graphitic materials. These domains of sp^3 hybridized atoms are suggested to act as diamond nucleation sites and lower the nucleation barrier. So, the electronic and transport properties of graphitic carbon nanomaterials can be considerably modified by the introduction of defects in them
- Topological defects like non-hexagonal rings introduces a curvature into the carbon nanostructures, and this curvature results in hybridization changes from sp^2-like to sp^3-like, locally. This, sp^3-like bonding increases with increasing curvature. For example carbon atoms in fullerenes inevitably have almost 10% of sp^3-like character. In addition, highly curved CNTs are found to be more reactive.
- Some specific defects known as Stone-Wales defects in sp^2 carbon materials are nucleation points for the growth and expansion of sp^2-matrix itself, in contrast to sp^3-like structural defects. Basically, the Stone-Wales defects maybe considered as seeds for the rearrangement of the graphitic lattice. It is also found that these particular defects can be employed to connect two individual CNTs, and the resultant tube will have different electronic density of states from its parent CNTs. It exhibits a sudden increase in the density of states at the Femi-level.

2. Electron irradiation induced structural changes in Multi- Walled Carbon Nanotubes:

Graphite and diamond are most common forms of carbon allotropes. They both are well-known for their individual applications in real life [1–3]. Graphite is the thermodynamically stable allotrope at macroscopic scale [4,5], and forms at ambient conditions, while diamond is the metastable one [4] and is known to form at very high pressures and temperatures [6]. First synthetic diamond was obtained using high pressure high temperature (HPHT) method by pressurizing graphite up to 8-10 GPa along with the temperatures above 2000^{o}C [7]. Despite the commercial success of synthetic diamond formation techniques, the conversion of graphite and graphite like materials into diamond continues to be of fundamental interest, particularly at microscopic sizes and nucleation stage [8,9].

Further going down in size and dimensionality, like chemical vapor deposition (CVD) films, diamond coatings and nanodiamond synthesis, things become really interesting. Unlike the HPHT process, the CVD approach produces diamond films at relatively low pressures. CVD synthesis is performed at very low pressures (2.6-4 kPa), with substrate temperatures about 900°C. The most widely accepted explanation for how diamond forms in the CVD process at low pressures is the preferential etching of graphite by hydrogen as compared to the diamond.

At first, the hypothesis of self-compression seems plausible but not conclusive, because direct pressure measurements are not possible under in-situ irradiation. According to this hypothesis, a certain surface tension builds up on the surface of onions because of diminishing surface area primarily due to the atoms being knocked out by high energy electrons. However, in reality it has been reported that the pressure at the cores is higher than that of at the surface. i.e., the core is acting like a source of pressure, which is inconsistent because the pressure is meant to build up at the surface and supposed to get transmitted to the core through the covalently bonded strong graphitic shells. Additionally, there is a large disagreement in the reported pressure values that are believed to prevail at the cores of the onions; for example ranging from 10 GPa to 100 GPa. Furthermore, the ability of carbon shells to transmit the pressure is not established. However, utilizing TEM alone makes it impossible to investigate both the presence of high pressure at the onion's core or the role of curvature in altering the bonding nature to facilitate the diamond formation. Experiments specially designed in terms of correct choice of materials and experimental conditions are lacking, thereby exposing a gap in representing the conditions and the mechanism of the nucleation of diamond in general, more specifically under electron i

3. Experimental methods:

3.1. RF plasma oxidation:

Core (iron oxide-diameter 5 nm)/shell (a-C – diameter 20 nm) samples were prepared by lamp black method. The synthesis details are described in the chapter 2. Radio frequency (RF) plasma oxidation is performed on core (iron oxide) – shell (a-C) sample to etch out the carbon shell and get only iron oxide particles to use as a pressure marker without shell.

3.2. High pressure X-ray diffraction:

High-pressure X-Ray Diffraction (XRD) experiments were performed at BL11, Indus-2. RRCAT, Indore, using a Diamond Anvil Cell (DAC). The DAC employs a pair of diamonds with culet size ~500 µm each. Stainless Steel gasket (initial thickness ~250 µm) of indented thickness ~140 µm and chamber dia ~250 µm was used to contain (i) sample, (ii) pressure calibrant (silver), and (iii) Methanol: Ethanol (4:1) as pressure transmitting medium. The XRD studies were performed in an angle dispersive mode (λ=0.633 Å). The operating parameters of the synchrotron were 2.5 GeV and 150mA. The high-pressure XRD study has been conducted on both shell removed sample as well as core-shell sample.

3.3. High pressure Raman spectroscopy:

High-pressure Raman spectroscopy measurements were carried out at room temperature using M/S Renishaw (model InVia) Raman spectrometer with 514 nm DPSS laser as an excitation source. Raman measurements were carried out to investigate any possible structural/configurational changes in carbon shell under applied high pressure. For this we have carried out Raman measurements by loading sample (core-shell Fe_2O_3/CB NPs) along with the pressure transmittance medium as Methanol: Ethanol (4:1). Small ruby crystals were also placed inside the gasket to measure the pressure inside the cell. The pressure is calibrated from the R1line emission of ruby crystals [5].

4. Results and discussion:

The starting CB sample has iron oxide core that is surrounded by spherical carbon shell as observed from transmission electron micrographs, also discussed in chapter 3. The carbon shell consists of concentric graphitic layers with defects and stacking faults. To study the carbon shell's pressure transmission behavior from the surface towards its core, the iron oxide nanoparticles located at the core were used as marker to see any departure from the ideal compression at the pressure outside the shell. In order to obtain the sample consisting of iron oxide only inside the carbon shells and free of any iron oxide outside the shells (decorated on the shells), we have performed an acid treatment. CB is mixed the in the hydro-chloric acid (HCl). The HCl cannot enter inside the carbon shells [6] and interact with the iron oxide particles inside the core, whereas it dissolves the free iron oxide outside the shells and results in the formation of a solution in green color. This process was repeated with drying until no green color solution was visible and all the free iron oxide outside the carbon shells was removed. By doing this, we have obtained the core-shell CB samples with no free iron oxide outside of the carbon shells. In this way, we ensure that only the same core iron oxide particles inside the a-C shells are used as the control sample to probe the true lattice compression in both the configurations. For this we have removed the carbon shell using plasma etching rather than by thermal oxidation as it can result in the unwanted structural transformations and agglomeration of these iron oxide particles. So we prepared two systems, (i) core (γ-Fe_2O_3)shell (C) sample and (ii) shell removed sample (control sample).

4.1. X-ray diffraction:

High-pressure XRD experiments are performed on the core-shell sample and shell-removed iron oxide nanoparticles. These samples are investigated up to around 6 GPa pressure. **Fig. 5.1** shows the XRD patterns of both these samples at various pressures. The reflections from silver (pressure calibrant) [ICDD card number: 00-004-0783] and Fe_2O_3 nanoparticles [JCPDS card number: 391346] are marked in these patterns. The iron oxide signal is very weak and nearly undetectable after ~ 6 GPa of pressure because of a low sample content the DAC. As the carbon shell is very defective it doesn't contribute to any peaks in the XRD pattern.

From Fig. 4.1, with increasing pressure, in both the core-shell and control samples, a down shift in the peak position (*d*-spacing) of iron oxide nanoparticles is seen. However, the iron oxide inside the carbon shell required higher pressures to attain the same d-spacings (for (*311*) reflection of Fe_2O_3) as compared to the control sample which attains these d-spacings at lower pressures. In other words, to obtain same *d*-spacing the core-shell sample needs higher pressure than it is required for control sample. For instance, the iron oxide encapsulated by the carbon shells attained a *d*-spacing of 2.497Å at a pressure of 5.4 GPa, whereas the control sample did the same at a pressure of 2.8 GPa itself. The plot in Fig. 4.1 depicts how the d-spacing of iron oxide changes for both samples as a function of applied pressure. Here, it is evident that, for the same applied pressure range, the line slope for the control sample is steeper than that of the core-shell sample. This finding suggests that, in comparison to the control sample, the iron oxide core with encompassing CB shell was subjected to a pressure less than that was applied.

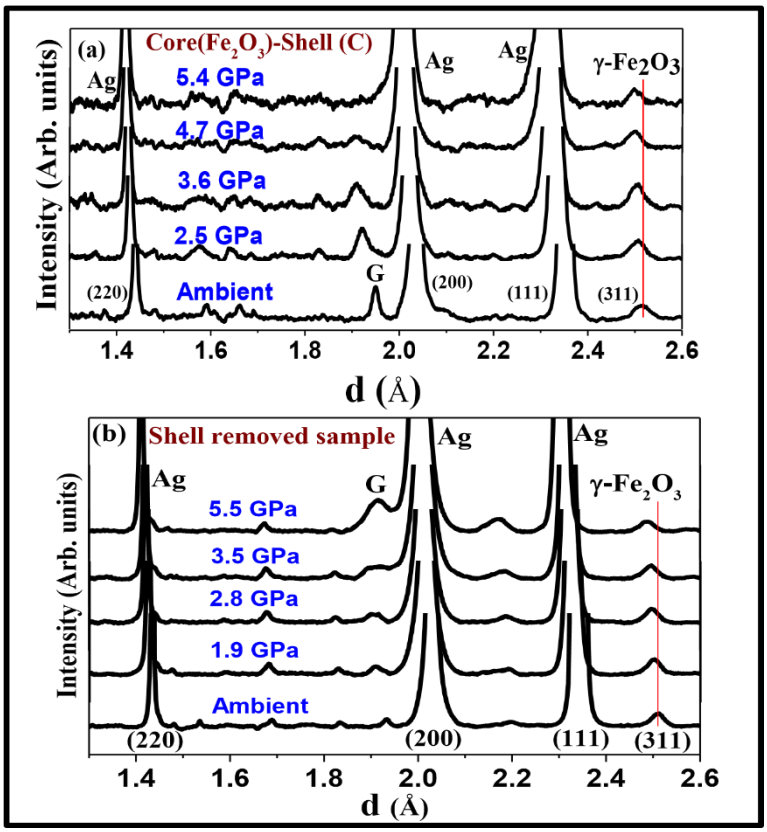

Fig. 4.1: The high pressure XRD patterns of (a) core-shell and (b) shell removed samples. The peaks of silver and iron oxide are marked. Peak due to the stainless steel gasket is denoted by 'G' in the figure.

In addition, pressure versus volume patterns for both the samples plotted in order to calculate the apparent bulk moduli of iron oxide (shown in **Fig. 5.3**) in both cases. The bulk moduli are computed by fitting the data using Birch-Murnaghan 3rd order equation [7, 8]. It is found that the bulk modulus of iron oxide encompassed by carbon shell (253.6 ± 5.6 GPa) more than that of control sample (184.3 ± 3.2 GPa). The reported range of bulk modulus of nanocrystalline Fe_2O_3 is 143-262 GPa, and is typically size dependent [9]. So, in order to ensure that the marker (Fe_2O_3) in both the samples is same, plasma oxidation is chosen to remove the carbon shell instead of thermal oxidation. This precaution is taken to prevent any changes in particle size due to agglomeration and phase transformations in Fe_2O_3 which could be triggered by thermal oxidation[10,11]. By doing this, it is ensured that the measurement of the marker (Fe_2O_3) core particles has contribution from the actual pressure applied onto it.

This observation emphasizes the fact that the iron oxide core encapsulated by CB shell is indeed is being subjected to a pressure less than that was applied, in comparison to the control sample. This in turn implies that the carbon shells are not completely transmitting the applied high pressure, rather they result in the reduction of effective pressure that get transferred to the iron oxide core.

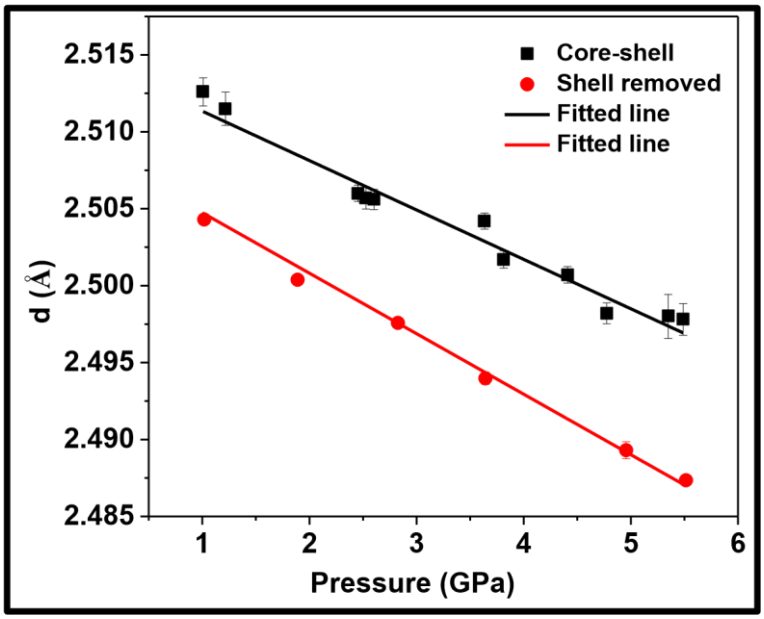

Fig. 4.2: Spacing d_{311} of core γ-Fe_2O_3 as a function of pressure for with and without a-C shell. Continuous lines show linear curve fit to the experimental data. The fall in the d-spacing in case of shell removed sample is steeper than that of core-shell sample.

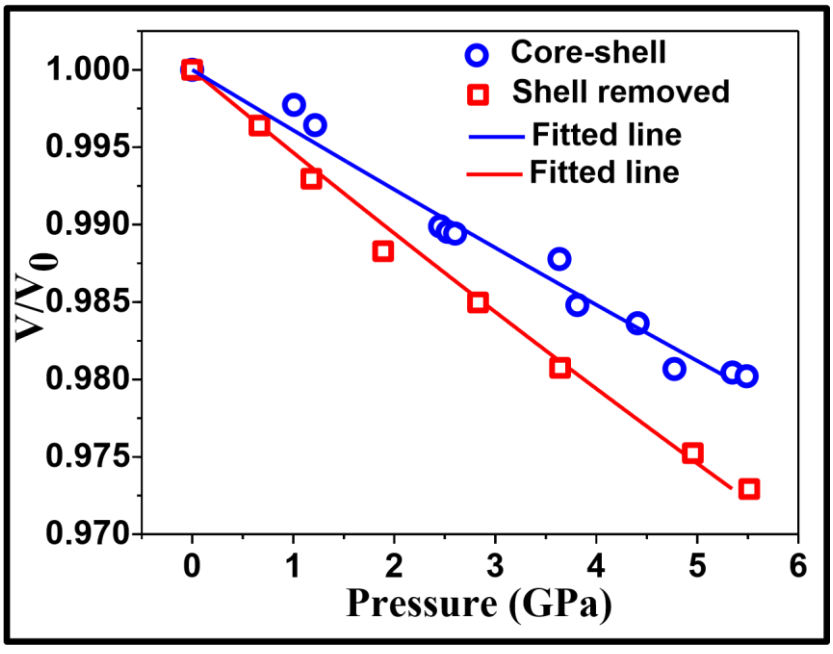

Fig. 4.3: Pressure versus volume plot of both core-shell and shell-removed samples. The plots are fitted with Birch-Murnagan 3rd order equation to obtain the bulk modulus of iron oxide in both the samples. Continuous lines show Birch-Murnagan curve fit to the experimental data.

5. Raman spectroscopy:

Furthermore, Raman spectroscopic measurements are carried out on core-shell sample in order to study the vibrational properties of carbon shell under high pressure. Raman spectroscopy is an effective method that is non-destructive tool for characterizing carbon-based materials [10]. Representative Raman spectrum of starting sample before compression is shown in **Fig. 5.1**. The G-peak at 1576 cm^{-1} results from the in-plane stretching modes of carbon atoms that are bonded with sp^2-hybridization, while the D-band at 1348 cm^{-1} is a defect-induced peak. Another peak at 1608 cm^{-1} is also a defect induced peak and denoted as D' peak. Two small and broad peaks at around 1200 (D4-peak) and 1500 cm^{-1}(D3-peak) are observed. Some reports attributed the D4 peak to sp^3 content in the samples, whereas some other reports attributed it to aliphatic moieties connected to carbon atoms in the graphitic sheets [13,14]. The D3 peak appears due to the presence of amorphous carbon in the samples [15]. The second order Raman spectra consist of 4 peaks around 2500 (D+D"), 2690 (2D), 2925 (D+G) and 3177 cm^{-1} (2D'), respectively.

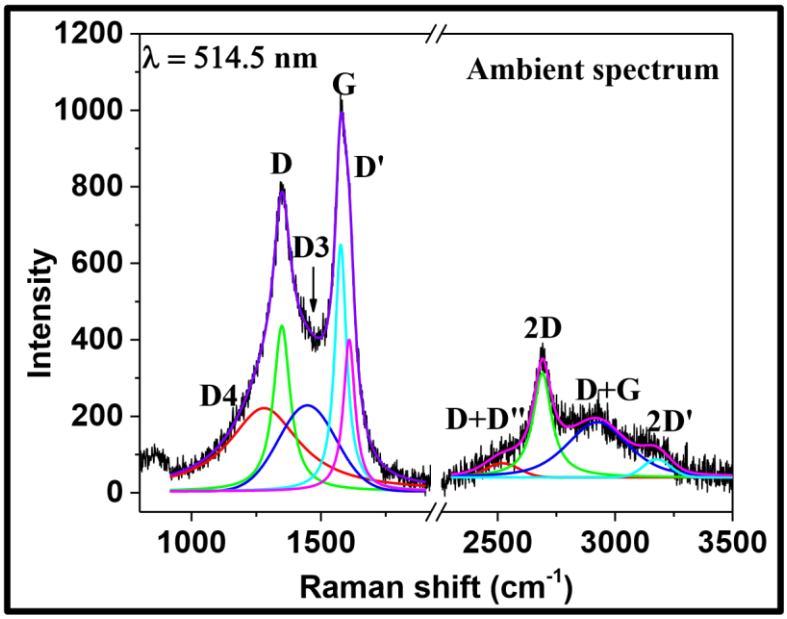

Fig. 5.1: Raman spectrum of starting sample (core-shell) before compression. The plot shows the first order (up to ~2000cm^{-1}) Raman modes and beyond that the combination modes of graphitic carbon. The corresponding peaks are marked.

However, as discussed in chapter 2, while applying pressure, the defect induced D-peak gets obscured by the over-whelming Raman intensity from diamond and could not record. So, the analysis of spectra has been restricted to beyond this range. **Fig. 5.2** depicts the evolution of Raman spectra of this core-shell sample from ambient pressure to the applied high pressure of ~25 GPa (for loading and unloading). It is evident from **Fig. 5.2(a)** that as the pressure increases the G-peak becomes broader and gets blue shifted, indicating the hardening of carbon-carbon in-plane interactions. A new peak seems to appear in the depicted range in **Fig. 5.2**. This peak is actually D3 that gets blue shifted with pressure eventually and comes within the investigated range at about 18 GPa.

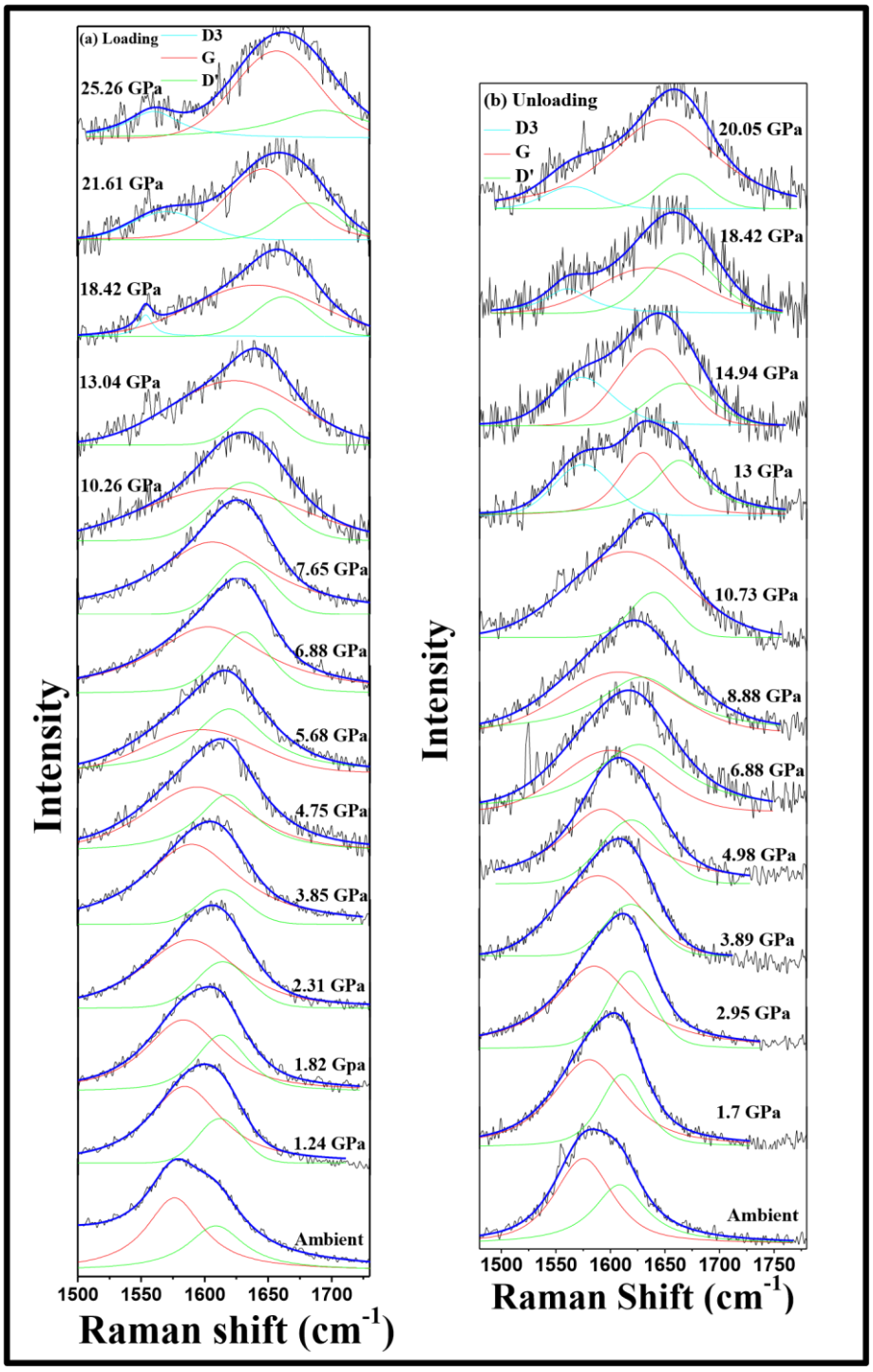

Fig. 5.5: Pressure dependence of Raman G-peak and D'-peak of core-shell sample during loading (a) and unloading (b). The respective pressure values are given along with the spectra. As the pressure is increasing, the G-peak gets broadened and shifts towards higher wavenumbers. During the unloading, the fully recovered Raman spectrum implies that the pressure induced changes are nearly reversible.

REFERENCES:

1. S. Nasir, M.Z. Hussein, Z. Zainal, N.A. Yusof, Carbon-Based Nanomaterials/Allotropes: A Glimpse of Their Synthesis, Properties and Some Applications, Mater. 2018, Vol. 11, Page 295. 11 (2018) 295. https://doi.org/10.3390/MA11020295.
   A. Prosvetov, Ion-beam induced modifications of structural and thermophysical properties of graphite materials, Tech. Univ. Darmstadt. Ph.D. Thesis (2020). https://tuprints.ulb.tudarmstadt.de/id/eprint/13253.
2. X. Chen, X. Wang, D. Fang, A review on C1s XPS-spectra for some kinds of carbon materials, Fullerenes, Nanotub. Carbon Nanostructures 28 (2020) 1048–1058. https://doi.org/10.1080/1536383X.2020.1794851.

3. M.L. Cohen, Calculation of bulk moduli of diamond and zinc-blende solids, Phys. Rev. B 32 (1985) 7988. https://doi.org/10.1103/PhysRevB.32.7988.
4. P.D. Ownby, X. Yang, J. Liu, Calculated X-ray Diffraction Data for Diamond Polytypes, J. Am. Ceram. Soc. 75 (1992) 1876–1883. https://doi.org/10.1111/J.11512916.1992.TB07211.X.
5. F.P. Bundy, J.S. Kasper, Hexagonal Diamond—A New Form of Carbon, J. Chem. Phys. 46 (1967) 3437. https://doi.org/10.1063/1.1841236.
6. C.G. Salzmann, B.J. Murray, J.J. Shephard, Extent of stacking disorder in diamond, Diam. Relat. Mater. 59 (2015) 69–72. https://doi.org/10.1016/J.DIAMOND.2015.09.007.
7. S. Ferro, Synthesis of diamond, J. Mater. Chem. 12 (2002) 2843–2855. https://doi.org/10.1039/B204143J.
8. T.W. Zerda, W. Xu, A. Zerda, Y. Zhao, R.B. Von Dreele, High pressure Raman and neutron scattering study on structure of carbon black particles, Carbon 38 (2000) 355–361. doi:10.1016/S0008-6223(99)00111-6.
9. Y. Lin, L. Zhang, H. Mao, P. Chow, Y. Xiao, M. Baldini, J. Shu, W.L. Mao, Amorphous Diamond: A High-Pressure Superhard Carbon Allotrope, Phys. Rev. Lett. 107 (2011) 175504. doi:10.1103/PhysRevLett.107.175504.
10. H.K. Poswal, S. Karmakar, P.K. Tyagi, D.S. Misra, E. Busetto, S.M. Sharma, A.K. Sood, High-pressure behavior of Ni-filled and Fe-filled multiwalled carbon nanotubes, Phys. Status Solidi B 244 (2007) 3612–3619. doi:10.1002/pssb.200642608.
11. P.K. Yadav, M. Kumar, R.K. Gupta, M. Sinha, J.A. Chakera, M.H. Modi, Refurbishment of an Au-coated toroidal mirror by capacitively coupled RF plasma discharge, J.
12. Synchrotron Radiat. 26 (2019) 1152–1160. doi:10.1107/S1600577519003485.
13. J.A. Xu, H.K. Mao, P.M. Bell, High-Pressure Ruby and Diamond Fluorescence: Observations at 0.21 to 0.55 Terapascal, Science 232 (1986) 1404–1406. doi:10.1126/SCIENCE.232.4756.1404.
14. P.-X. Hou, C. Liu, H.-M. Cheng, Purification of carbon nanotubes, Carbon 46 (2008) 2003– 2025. doi:10.1016/j.carbon.2008.09.009.
15. J.Z. Jiang, J. Staun Olsen, L. Gerward, S. MØrup, Enhanced bulk modulus and reduced transition pressure in γ-Fe2O3 nanocrystals, Europhys. Lett. 44 (1998) 620–626. doi:10.1209/epl/i1998-00563-6.
16. J. Zhao, L. Guo, J. Liu, Y. Yang, R.Z. Che, L. Zhou, High bulk modulus of nanocrystal γFe2O3 with chemical dodecyl benzene sulfonic decoration under high pressure, Chinese Phys. Lett. 17 (2000) 126–128. doi:10.1088/0256-307X/17/2/018.